Calcium entry into stereocilia drives adaptation of the mechanoelectrical transducer current of mammalian cochlear hair cells

Laura F. Corns[a,1], Stuart L. Johnson[a,1], Corné J. Kros[b,c], and Walter Marcotti[a,2]

[a]Department of Biomedical Science, University of Sheffield, Sheffield S10 2TN, United Kingdom; [b]Sussex Neuroscience, School of Life Sciences, University of Sussex, Falmer, Brighton BN1 9QG, United Kingdom; and [c]Department of Otorhinolaryngology, Head and Neck Surgery, University Medical Center Groningen, University of Groningen, 9700 RB, Groningen, The Netherlands

Edited by A. J. Hudspeth, Howard Hughes Medical Institute, The Rockefeller University, New York, NY, and approved August 22, 2014 (received for review May 28, 2014)

Mechanotransduction in the auditory and vestibular systems depends on mechanosensitive ion channels in the stereociliary bundles that project from the apical surface of the sensory hair cells. In lower vertebrates, when the mechanoelectrical transducer (MET) channels are opened by movement of the bundle in the excitatory direction, Ca^{2+} entry through the open MET channels causes adaptation, rapidly reducing their open probability and resetting their operating range. It remains uncertain whether such Ca^{2+}-dependent adaptation is also present in mammalian hair cells. Hair bundles of both outer and inner hair cells from mice were deflected by using sinewave or step mechanical stimuli applied using a piezo-driven fluid jet. We found that when cochlear hair cells were depolarized near the Ca^{2+} reversal potential or their hair bundles were exposed to the in vivo endolymphatic Ca^{2+} concentration (40 μM), all manifestations of adaptation, including the rapid decline of the MET current and the reduction of the available resting MET current, were abolished. MET channel adaptation was also reduced or removed when the intracellular Ca^{2+} buffer 1,2-Bis(2-aminophenoxy)ethane-*N*,*N*,*N*′,*N*′-tetraacetic acid (BAPTA) was increased from a concentration of 0.1 to 10 mM. The findings show that MET current adaptation in mouse auditory hair cells is modulated similarly by extracellular Ca^{2+}, intracellular Ca^{2+} buffering, and membrane potential, by their common effect on intracellular free Ca^{2+}.

Hearing and balance depend on the transduction of mechanical stimuli into electrical signals. This process depends on the opening of mechanoelectrical transducer (MET) channels located at the tips of the shorter of pairs of adjacent stereocilia (1), which are specialized microvilli-like structures that form the hair bundles that project from the upper surface of hair cells (2,3). Deflection of hair bundles in the excitatory direction (i.e., toward the taller stereocilia) stretches specialized linkages, the tip-links, present between adjacent stereocilia (3–5), opening the MET channels. In hair cells from lower vertebrates, open MET channels reclose during constant stimuli via an initial fast adaptation mechanism followed by a much slower, myosin-based motor process, both of which are driven by Ca^{2+} entry through the channel itself (6–13). In mammalian auditory hair cells, MET current adaptation seems to be mainly driven by the fast mechanism (14–16), although the exact process by which it occurs is still largely unknown. The submillisecond speed associated with the adaptation kinetics of the MET channels in rat and mouse cochlear hair cells (17, 18) indicates that Ca^{2+}, to cause adaptation, has to interact directly with a binding site on the channel or via an accessory protein (16). However, a recent investigation on rat auditory hair cells has challenged the view that Ca^{2+} entry is required for fast adaptation, and instead proposed an as-yet-undefined mechanism involving a Ca^{2+}-independent reduction in the viscoelastic force of elements in series with the MET channels (19). In the present study, we further investigated the role of Ca^{2+} in MET channel adaptation in mouse cochlear hair cells by deflecting their hair bundles using a piezo-driven fluid jet, which is believed to produce a more uniform deflection of the hair bundles (20–23) compared with the piezo-driven glass rod (19, 24).

Results

MET Currents Recorded in Mouse Outer and Inner Hair Cells. MET currents were elicited by displacing the hair bundles of both outer hair cells (OHCs) and inner hair cells (IHCs) with a piezoelectric fluid jet stimulator (20–22). The fluid jet was preferred to a rigid probe (17, 19) because it does not require any direct contact with the stereocilia, which could affect their resting position and also damage some of the interciliary links (16). Unless the shape of the probe is perfectly matched to that of the V- or U-shaped bundle of the OHCs or IHCs, respectively, this method would also lead to nonuniform displacement of individual stereocilia (16, 25, 26). Such uniformity is achieved with fluid jet stimulation (Fig. S1). MET currents were elicited from 14 OHCs and 7 IHCs of postnatal day 6 (P6) to P9 mice (Fig. 1 *A*–*C*) in response to a sinewave stimulus. Upon moving their bundles in the excitatory direction (i.e., toward the taller stereocilia using positive driver voltages), large inward currents flowed at negative membrane potentials (−121 mV; Fig. 1 *A*–*C*). The resting MET current was shut off in the inhibitory phase of the stimulus. With membrane depolarization, the MET current decreased in size at first and then reversed near 0 mV (Fig. 1*C*), in agreement with the

Significance

In the inner ear, the sensory receptor cells (hair cells) signal reception of sound. They do so by converting mechanical input, due to sound waves moving the hair bundles on these cells, into electrical current through ion channels situated at the tips of the bundles. To keep the receptors operating at their maximum sensitivity, the current declines rapidly, a process known as adaptation. In nonmammalian vertebrates, Ca^{2+} ions entering the mechanosensitive ion channels drive adaptation, but it has been questioned whether this mechanism applies to mammals. We show that adaptation in mammalian cochlear hair cells is, as in other vertebrates, driven by Ca^{2+} entry, demonstrating the importance of this process as a fundamental mechanism in vertebrate hair cells.

Author contributions: L.F.C., S.L.J., C.J.K., and W.M. designed research; L.F.C., S.L.J., and W.M. performed research; L.F.C., S.L.J., and W.M. analyzed data; and L.F.C., S.L.J., C.J.K., and W.M. wrote the paper.

The authors declare no conflict of interest.

This article is a PNAS Direct Submission.

Freely available online through the PNAS open access option.

[1]L.F.C. and S.L.J. contributed equally to this work.

[2]To whom correspondence should be addressed. Email: w.marcotti@sheffield.ac.uk.

This article contains supporting information online at www.pnas.org/lookup/suppl/doi:10.1073/pnas.1409920111/-/DCSupplemental.

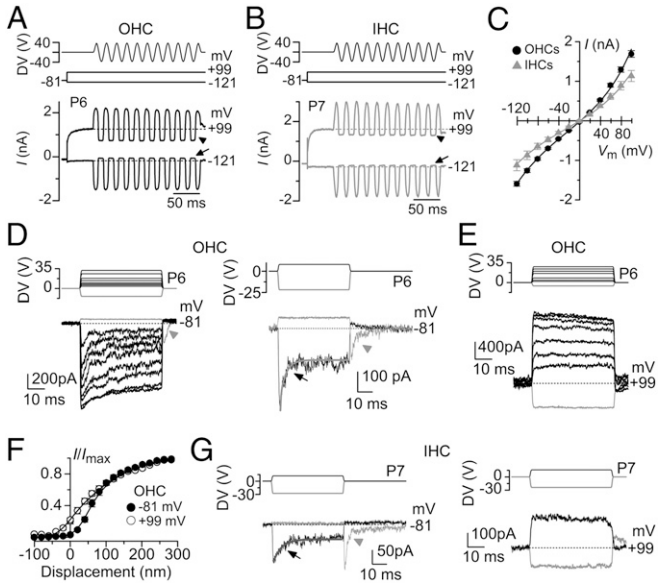

Fig. 1. MET currents in mouse cochlear OHCs and IHCs. (*A* and *B*) Saturating MET currents recorded from an OHC (*A*) and an IHC (*B*) in response to 50-Hz sinusoidal force stimuli to the hair bundles at membrane potentials of −121 and +99 mV. The driver voltage (DV) signal of ±35 V to the fluid jet is shown above the traces (positive deflections of the DV are excitatory). The arrows and arrowheads indicate the closure of the transducer channels, i.e., disappearance of the resting current, during inhibitory bundle displacements at −121 mV and +99 mV, respectively. Dashed lines indicate the holding current. (*C*) Peak-to-peak MET current–voltage curves obtained from 14 OHCs and 7 IHCs (P6–P9) using 1.3 mM extracellular Ca^{2+}. The fits through the current–voltage curves are according to a single-energy-barrier model (Eq. **1**):

$$I(V) = k[\exp((1-\gamma)(V-V_r)/V_s) - \exp(-\gamma(V-V_r)/V_s)],$$

where k is a proportionality constant, V_r is the reversal potential, V_s is a measure for the steepness of the rectification, and γ is the fractional distance within the membrane's electrical field of an energy barrier, as measured from the outside (20). The values of the fits are as follows: OHCs: k = 444 pA, V_r = 1.3 mV, V_s = 38 mV, γ = 0.41; IHCs: k = 323 pA, V_r = 0.2 mV, V_s = 40 mV, γ = 0.42. (*D*) MET currents recorded at −81 mV (*Lower*) from an OHC elicited by force-step stimuli (*Upper*). Positive DVs of 50-ms duration (excitatory direction) elicited inward MET currents that declined or adapted over time (arrow in *Right*). Holding current: −90 pA. A small transducer current was present at rest, and inhibitory bundle displacements turned this off (gray traces). Upon termination of the inhibitory stimulus, the MET current showed evidence of rebound adaptation (arrowheads). *Right* shows double-exponential fit to the MET current decay (*Results*). The bundle movement for the inhibitory and excitatory step was −221 and 81 nm, respectively. In this and the following figures, bundle motion during fluid jet stimulation was estimated by using a conversion value of 10.1 nm/V obtained with a photodiode system (*Materials and Methods* and Fig. S2). (*E*) MET currents recorded at +99 mV from the same OHC as in *D*. Holding current: +861 pA. Note that all manifestations of transducer current adaptation [current decline during excitatory stimuli and rebound following inhibitory stimuli (*D*)] were absent at +99 mV, and the resting current was increased. (*F*) Normalized peak MET current recorded from seven OHCs at the holding potential of −81 mV and during a step to +99 mV as a function of bundle displacement. Note the leftward shift and shallower slope at +99 mV. The resting open probability between −81 mV (0.033 ± 0.004; n = 7) and +99 mV (0.22 ± 0.02) was found significantly different (paired t test; $P < 0.0002$). The relation between the normalized MET current and hair-bundle displacement was fitted by using a second-order Boltzmann function (Eq. **2**):

$$I/I_{max} = 1/\left(1+\exp(a_2(x_2-x)) * (1+\exp(a_1(x_1-x)))\right).$$

Fits to the data points were as follows: at −81 mV: I_{max} = −1,024 pA, a_1 = 0.044 nm^{-1}, a_2 = 0.015 nm^{-1}, x_1 and x_2 = 51 nm; at +99 mV: I_{max} = 1,744 pA, and the other parameters were as at −81 mV, except for x_1 = −10 nm, indicating a leftward shift of 61 nm. (*G*) MET currents recorded at −81 mV (*Left*) and +99 mV (*Right*) from an IHC elicited by force-step stimuli (*Upper*) as in *D*. Holding current: −132 pA (*Left*) and +1,268 pA (*Right*). Note that adaptation was absent at +99 mV.

nonselective permeability of MET channels to cations (27), to become outward, with a larger resting current at positive potentials. We then stimulated the stereocilia of hair cells using force steps to better investigate the adaptation properties of the MET current (Fig. 1 *D*–*G*). Upon moving the bundles in the excitatory direction and at −81 mV, adaptation- or time-dependent decline of the MET current in OHCs occurred for small driver voltages that produce nonsaturating bundle displacements (72 ± 7 nm, n = 14; approximately halfway through the bundle operating range shown in Fig. 1*F*). Adaptation exhibited a fast time constant (0.65 ± 0.08 ms; n = 14; contributing 57.3% of the total extent of adaptation described by the exponential fit) and a slow time constant (16.9 ± 2.4 ms; contributing the residual 42.7%; n = 14; arrow in Fig. 1 *D*, *Right*). Inhibitory hair bundle deflection (negative driver voltage) shut off the small fraction of current flowing at rest, with the offset of large inhibitory steps causing a transient rebound inward MET current (downward dip indicated by the arrowheads in Fig. 1*D*). All of these manifestations of MET current adaptation were absent when stepping the membrane potential from –81 mV to a positive value (+99 mV: Fig. 1*E*), which is near the Ca^{2+} equilibrium potential and strongly reduces Ca^{2+} entry into the MET channels. This finding is consistent with Ca^{2+} entry driving adaptation as demonstrated in hair cells from lower vertebrates (9, 10). Additional evidence for the presence of MET current adaptation is the channels' increased resting open probability when Ca^{2+} influx into the stereocilia is decreased (9, 12, 28, 29), which was evident in OHCs at +99 mV (Fig. 1 *A* and *E*; see also Fig. 2*C*). This finding is also highlighted by the different shapes of the plots describing the relation between the mean peak MET current and bundle displacement (Fig. 1*F*; for driver voltage to bundle displacement conversion using a pair of photodiodes, see *Materials and Methods* and Fig. S2). The change in plot shape is consistent with a leftward shift upon depolarization in x1, the set point for the transition between the two closed states in a three-state channel model (10, 21) (see also the Fig. S3 legend). The same features were also seen in IHCs (Fig. 1 *B* and *G*), with adaptation evident for nonsaturating bundle displacements at −81 mV, with both fast (0.82 ± 0.31 ms; n = 6; contributing 36% of the total extent of adaptation) and slow (11.4 ± 4.3 ms; contributing the residual 64%) time constant components (Fig. 1 *G*, *Left*). At +99 mV, adaptation was abolished, and the resting MET current increased (Fig. 1 *G*, *Right*).

Modulation of MET Current Adaptation by Extracellular and Intracellular Calcium. To probe the direct dependence of MET current adaptation on intracellular Ca^{2+}, recordings from mouse cochlear hair cells were performed by using either low, endolymphatic extracellular Ca^{2+} (0.04 mM: see *Materials and Methods*) or different intracellular concentrations of the fast Ca^{2+} chelator 1,2-Bis (2-aminophenoxy)ethane-*N*,*N*,*N*′,*N*′-tetraacetic acid (BAPTA). Extracellular Ca^{2+} is known to block the current through the MET channels with a half-blocking concentration of 1 mM (12, 29). We found that reducing extracellular Ca^{2+} from 1.3 mM (Fig. 2*A*) to 0.04 mM (Fig. 2*B*) increased the MET current amplitude in both OHCs and IHCs, which stems from relief of the block by Ca^{2+} in the permeation pathway of the channel (30). Moreover, we observed a significantly (OHCs: $P < 0.0001$; IHCs: $P < 0.002$) increased resting open probability of the MET current when lowering the extracellular Ca^{2+} from 1.3 to 0.04 mM Ca^{2+} at –81 mV (Fig. 2 *A*–*C*), which is similar to that obtained when the membrane potential of both OHCs and IHCs was depolarized to +99 mV (Fig. 2*C*). All of these findings are consistent with the idea that Ca^{2+} entering through the MET channels causes adaptation

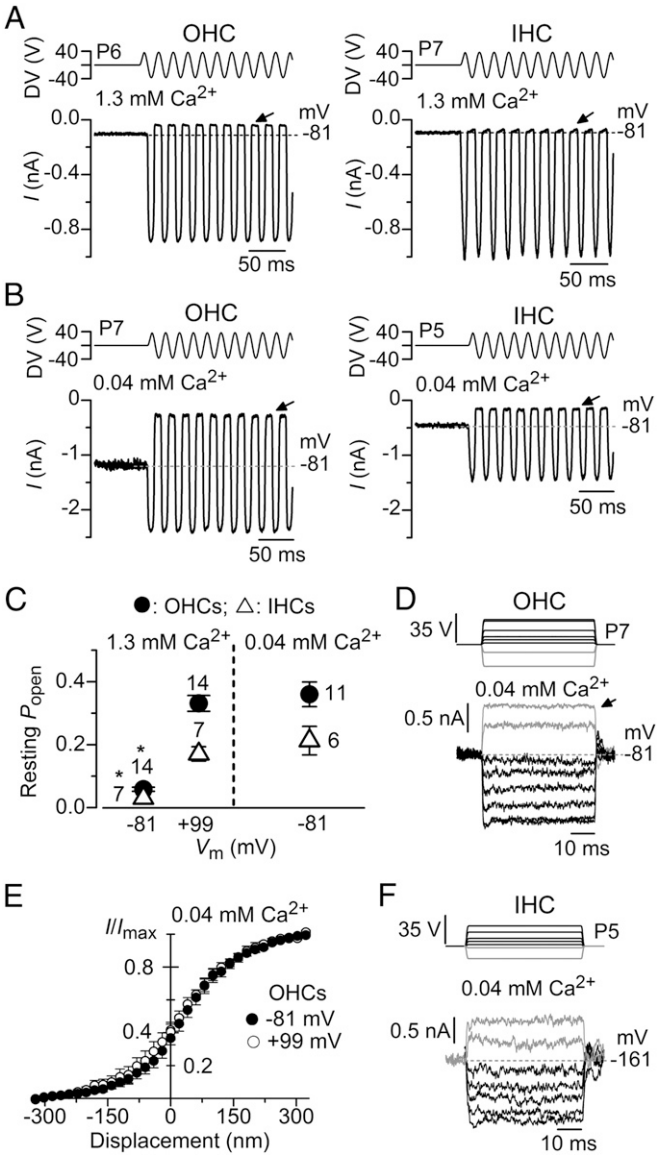

Fig. 2. Low extracellular Ca^{2+} removes MET current adaptation in mouse cochlear hair cells. (*A*) MET currents recorded from an OHC (*Left*) and an IHC (*Right*) in response to a 50-Hz sinusoidal force stimulus to the hair bundles at a membrane potential of −81 mV and in the presence of 1.3 mM extracellular Ca^{2+}. DV, driver voltage signal. The arrows indicate closure of the transducer channels and dashed lines the holding current. (*B*) MET currents recorded at −81 mV from an OHC and an IHC in the presence of endolymphatic Ca^{2+} (0.04 mM) instead of 1.3 mM Ca^{2+}. Note the larger resting MET current (difference between arrow and dashed line). (*C*) Resting open probability of the MET current obtained in OHCs and IHCs at −81 and +99 mV in 1.3 mM extracellular Ca^{2+} (*Left*) and at −81 mV in 0.04 mM extracellular Ca^{2+} (*Right*). The resting open probability was calculated by dividing the resting MET current (the difference between the current level before the stimulus, indicated by the dashed line, and the current level at the negative phase of the stimulus when all channels were closed) by the maximum peak-to-peak MET current. Number of cells is stated by the data points. (*D*) Step driver-voltages to the fluid jet (*Upper*) and MET currents recorded from an OHC at −81 mV in the presence of 0.04 mM extracellular Ca^{2+}. Holding current: −1,378 pA. Note that all manifestations of MET current adaptation (Fig. 1*D*) are absent. (*E*) Normalized peak MET current recorded from six OHCs at the holding potential of −81 mV and during a step to +99 mV as a function of bundle displacement in the presence of low extracellular Ca^{2+} (0.04 mM). Note the absence of the leftward shift in the MET current-bundle displacement upon stepping V_m to +99 mV. The resting open probability between −81 mV (0.37 ± 0.04, $n = 6$) and +99 mV (0.40 ± 0.05) was not significantly different (paired *t* test). (*F*) Step driver-voltages and MET currents recorded from an IHC at −161 mV in the presence of 0.04 mM extracellular Ca^{2+}. Holding current: −424 pA.

and that a reduced entry, in low Ca^{2+} conditions, significantly increases the open probability of the MET channels (9, 12, 28, 29). Different from 1.3 mM Ca^{2+} (Fig. 1*D*), low, endolymphatic extracellular Ca^{2+} removed MET current adaptation in response to displacement steps at −81 mV in six of nine OHCs investigated (Fig. 2*D*). In the three OHCs showing some residual adaptation, it was best fitted with a single exponential of 2.0 ± 0.6 ms ($n = 3$). In six OHCs in which step responses were recorded in 0.04 mM Ca^{2+} at membrane potentials of both −81 and +99 mV, the plots describing the relation between the mean peak MET current and bundle displacement were already shifted to the left at negative potentials (compare Fig. 2*E* with Fig. 1*F*), resulting in a large resting open probability of the MET channels. To mimic the in vivo physiological driving force generated by the endocochlear potential (31)—which is the potential generated between the endolymphatic and perilymphatic compartments [approximately +90 mV (32)]—we performed a few step-response experiments in 0.04 mM Ca^{2+} where IHCs were held at −161 mV. IHCs were preferred to OHCs for these experiments because they remained viable for longer when using such an extreme hyperpolarized holding potential. In three of four recordings, no time-dependent adaptation of the MET current was seen (Fig. 2*F*). One IHC showed a residual MET current decline with a time constant of 3.3 ms.

We then tested whether MET current adaptation was directly regulated by the free Ca^{2+} inside the stereocilia by changing the intracellular Ca^{2+} buffering capacity. Increasing the intracellular BAPTA from 0.1 mM to a range of concentrations up to 10 mM significantly augmented the resting open probability of the MET channel in both OHCs (one-way ANOVA: $P < 0.0001$; posttest between 0.1 and 5 mM BAPTA: $P < 0.01$; 0.1 and 10 mM BAPTA: $P < 0.01$) and IHCs (*t* test: $P < 0.02$ between 0.1 and 5 mM BAPTA) (Fig. 3 *A*–*C*). Similar to the findings in 1 mM EGTA (Fig. 1), MET current adaptation in response to non-saturating displacement steps (99 ± 12 nm, $n = 6$) was observed in 0.1 mM intracellular BAPTA (fast time constant: 0.82 ± 0.21 ms, $n = 6$; slow: 8.3 ± 1.5 ms) when OHCs and IHCs were held at −81 mV (Fig. 3 *D*, *Bottom*). Stepping the membrane potential to +99 mV removed MET current adaptation and increased the resting open probability (Fig. 3 *D*, *Middle*). In the presence of 5 mM intracellular BAPTA and at −81 mV, MET current adaptation was abolished or substantially reduced (in four of eight cells, the small MET current decline was best fitted with one time constant: 6.6 ± 2.8 ms) and the resting open probability increased (Fig. 3*E*), which is consistent with previous findings in lower vertebrates (10, 33). Similar results were obtained with 10 mM intracellular BAPTA in OHCs, which also showed very little change in the resting open channel probability when stepping the membrane potential V_m from −81 to +99 mV (Fig. 3*F*). In agreement with the findings in the presence of 0.04 mM Ca^{2+} (Fig. 2*E*), 5 and 10 mM intracellular BAPTA reduced or prevented, respectively, any further leftward shift in the mean peak MET current vs. bundle displacement relation when changing the membrane potential between −81 and +99 mV (Fig. 3*G*).

We confirmed whether the shift in the MET current-displacement relation was Ca^{2+}-dependent by using a paired-pulse protocol (7, 10, 19, 24, 34) in which two brief series of test steps (1.5 ms) were delivered, one before and the other toward the end of a nonsaturating adaptive step (20 ms) (Fig. 4). In the presence of a low intracellular BAPTA concentration (0.1 mM) and at −81 mV, the MET current-displacement relation obtained during the adaptive step was shifted along the displacement axis and was slightly steeper compared with that preceding

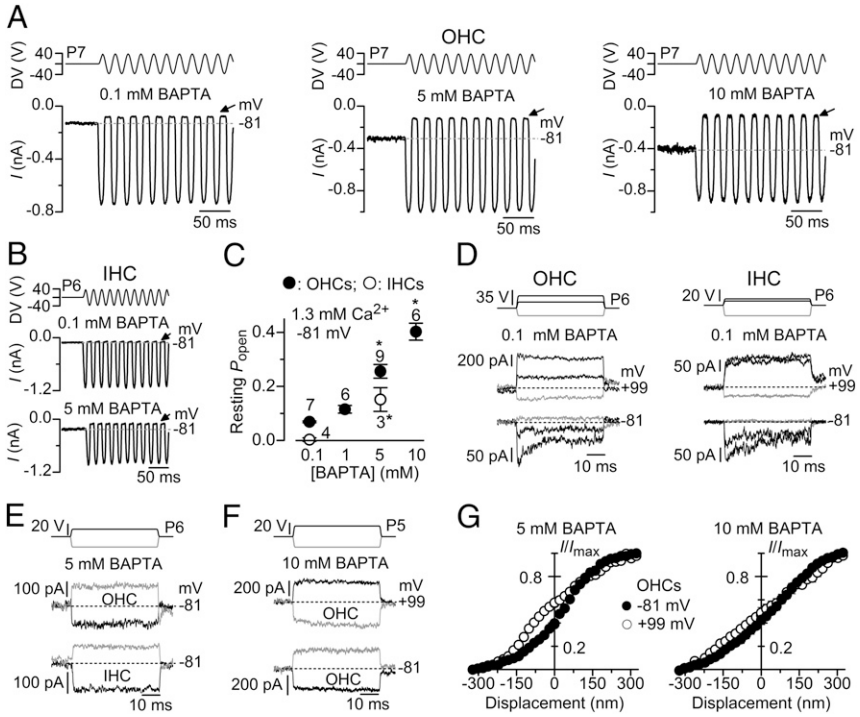

Fig. 3. MET current adaptation in mouse cochlear hair cells is removed by high intracellular BAPTA. (*A* and *B*) MET currents recorded from an OHC (*A*) and an IHC (*B*) in response to a 50-Hz sinusoidal force stimuli to the hair bundles at the membrane potential of −81 mV in the presence of different intracellular BAPTA concentrations. Recordings are as in Fig. 1 *A* and *B*. Note the increased resting MET current (difference between dashed lines and arrows) with increasing BAPTA concentration. (*C*) Resting open probability of the MET current recorded in OHCs and IHCs obtained at −81 mV and using different concentrations of intracellular BAPTA. (*D*) Step driver voltages to the fluid jet (*Top*) and MET currents recorded from OHCs (*Left*) and IHCs (*Right*) at −81 mV (*Bottom*) and +99 mV (*Middle*) in the presence of 0.1 mM BAPTA. Note that all manifestations of MET current adaptation were removed at +99 mV as shown in Fig. 1 *D* and *E* with 1 mM EGTA. (*E*) MET currents recorded from OHCs (*Middle*) and IHCs (*Bottom*) at −81 mV in the presence of 5 mM BAPTA. (*F*) MET currents recorded from an OHC at −81 and +99 mV in the presence of 10 mM BAPTA. As for 5 mM BAPTA (*E*), MET current adaptation was absent. (*G*) Normalized peak MET current recorded from OHCs at the holding potential of −81 and +99 mV as a function of bundle displacement in the presence of 5 mM ($n = 6$; *Left*) and 10 mM ($n = 6$; *Right*) intracellular BAPTA. Similar to the experiments in low Ca^{2+} (Fig. 2*E*), little (5 mM) or no (10 mM) leftward shift in the MET current-displacement relation was observed when cells were held at +99 mV in the presence of intracellular BAPTA. Resting open probability between −81 mV (5 mM: 0.39 ± 0.02, $n = 6$; 10 mM: 0.43 ± 0.04, $n = 6$) and +99 mV (5 mM: 0.57 ± 0.02; 10 mM: 0.48 ± 0.04) was only significantly different using 5 mM BAPTA (paired *t* test: $P < 0.001$).

the adaptive step in both OHCs (Fig. 4 *A*, *Bottom*) and IHCs (Fig. S4*A*). A similar, but larger, adaptive shift has been described in cochlear hair cells using a glass probe (19, 35). This larger adaptive shift is likely to be a direct consequence of the much wider operating range of bundle displacement obtained with the probe (~500 nm; refs. 19 and 35), compared with that elicited with the fluid jet (~200 nm) or when MET current was elicited by stimulation of the basilar membrane in vitro (<200 nm; ref. 36). The narrower bundle excursions obtained with the fluid jet are likely to be a more physiological estimation because they are a closer match to the in vivo measurements of basilar membrane motion that activate the MET channels (<100 nm; reviewed in ref. 16). If Ca^{2+} is the primary cause of adaptation, reducing its concentration near the MET channels should prevent the adaptive shift. In both OHCs and IHCs, we found that either stepping the membrane potential to +99 mV in the presence of 0.1 mM intracellular BAPTA (OHCs, Fig. 4*B*; IHCs, Fig. S4*B*) or keeping the cells at −81 mV but using 10 mM intracellular BAPTA (OHCs, Fig. 4*C*; IHCs, Fig. S4*C*) increased the MET channel open probability and prevented any significant shift along the displacement axis between the two test steps. This finding demonstrates that MET channel adaptation is under the direct control of Ca^{2+} at or near the channel.

Discussion

In this study, we have investigated the adaptation properties of the MET current in OHCs and IHCs of the mouse. By uniformly displacing the stereociliary bundle with a piezo-driven fluid jet, we show that all manifestations of MET current adaptation are removed or strongly reduced in endolymphatic extracellular Ca^{2+} (40 μM), high intracellular BAPTA (5 or 10 mM), and by preventing Ca^{2+} entry into the MET channels at depolarized membrane potentials. All these findings are consistent with the intracellular Ca^{2+} concentration in the stereocilia directly determining the adaptation state of the MET channel in mammalian cochlear hair cells. At endolymphatic extracellular Ca^{2+} concentrations, there is little evidence of rapid time-dependent adaptation (Fig. 2), even at a physiological driving force that includes the contribution of the endocochlear potential. However, given the differences with the in vivo situation, including the different temperature and the absence of the tectorial membrane, the very existence of adaptation in mammalian cochlear hair cells demonstrated here implies that MET channel adaptation may yet play a role in mammalian hearing. The resting MET current at endolymphatic Ca^{2+} concentrations is a lesser fraction of the total available current in IHCs (~20%) than in OHCs (~35%). This finding is suggestive of differences in their adaptation mechanisms, with the IHCs being in line with hair cells from other vertebrates (e.g., refs. 9 and 28) and the larger resting current in the OHCs optimizing the membrane time constant for electromotility (22). Our recordings with the fluid-jet stimulation revealed both fast and slow components of adaptation. The fact that both components of adaptation are similarly affected when changing either the extracellular Ca^{2+}

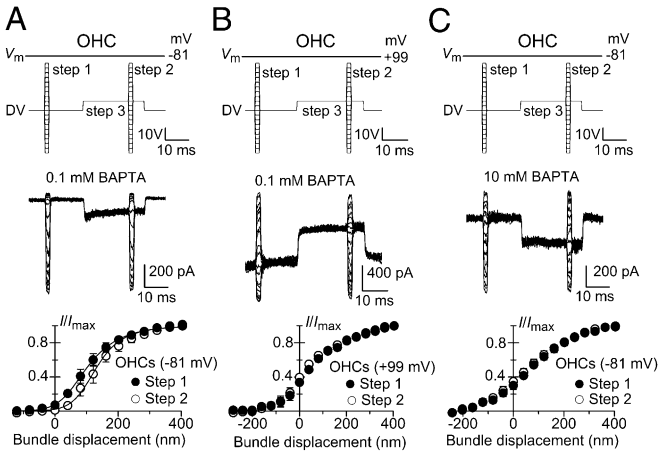

Fig. 4. Strong Ca^{2+} buffering and depolarization abolish the adaptive shift in response to a paired-pulse protocol. MET currents recorded from OHCs elicited by paired-pulse stimulation (*Upper*). Steps 1 and 2 were 1.5 ms in duration and elicited maximal MET currents. Step 3, the adaptive step (81 nm), was 20 ms in duration and elicited nonsaturating current to move the bundle to the most sensitive region of the current-displacement curve (Fig. 1 *D*–*G*). MET current recorded in P6 OHCs at −81 mV (*A*) and +99 mV (*B*) in the presence of intracellular 0.1 mM BAPTA and at −81 mV in 10 mM BAPTA (*C*). *Lower* shows the normalized peak MET currents recorded in P6–P7 OHCs before (step 1) and during (step 2) the adaptive step (step 3) as a function of bundle displacement in 0.1 mM (*A* and *B*, $n = 3$) and 10 mM intracellular BAPTA (*C*; $n = 7$). The bundle displacement at which 50% of the maximum MET current is activated was found to be significantly different between step 1 (100.4 ± 15.0 nm; $n = 3$) and step 2 (132.2 ± 18.7 nm) in 0.1 mM BAPTA and at −81 mV (*A*: paired *t* test: $P < 0.05$). No significant difference was found in all of the other experimental conditions (*B*: step 1: 48.3 ± 8.9 nm, $n = 3$; step 2: 32.2 ± 6.3 nm; *C*: step 1: 71.6 ± 11.9 nm, $n = 7$; step 2: 60.7 ± 17.9 nm). Data points in *A* were fitted using Eq. **2**: step 1 $I_{max} = -841$ pA, $a_1 = 0.020$ nm^{-1}, $a_2 = 0.013$ nm^{-1}, x_1 and $x_2 = 67$ nm; step 2 $I_{max} = -812$ pA, and the other parameters were as for step 1, except for $x_1 = 141$ nm, which show a Ca^{2+}-dependent adaptive shift of 74 nm to the right, in agreement with previous finding in turtle hair cells (10).

concentration or the intracellular Ca^{2+} buffering strength indicates that they have a quantitatively similar Ca^{2+} dependence and may thus originate from the same site, probably the MET channel. The changes in shape of the relation between MET current and bundle displacements upon depolarization (Fig. 1*F* and Fig. S3*C*) and during an adaptive step (Fig. 4*A* and Fig. S4*A*; ref. 35) are also hard to reconcile with adaptation being due to a process extrinsic to the channel, such as one driven by myosin motors (16).

The MET channel in hair cells is a cation channel with a high Ca^{2+} permeability (27). Although the nature of the MET channels is still unknown, recent findings have shown that transmembrane channel-like (TMC)1 and TMC2 proteins are likely candidate subunits (37). A crucial feature of the MET machinery is that, in response to a sustained deflection of the hair bundle, it adapts, so that the channel operating range is kept near its maximal sensitivity (14, 16). MET channel adaptation manifests as a time-dependent decline in the current amplitude during sustained bundle displacements and a reduced resting open channel probability, which is evident by the shift in the current-displacement relation. Previous studies on lower-vertebrate hair cells have demonstrated that transducer adaptation is regulated by Ca^{2+} entry into the stereocilia via the MET channel itself (6–13). However, it has recently been proposed that Ca^{2+}-dependent adaptation is not present in mammalian cochlear hair cells (19), which our findings contradict. The main difference between the two studies is the device used to displace the hair bundle: the fluid jet (present study) and rigid glass probe (19). The disadvantage of the rigid probe, compared with the fluid jet, is that it requires optimal vertical and angular positioning to produce a homogeneous displacement of the V- or U-shaped hair bundle of OHCs and IHCs, respectively. Because the glass probe may not contact some stereocilia, when the probe is displaced (16, 25), all stereociliary rows are initially deflected by viscous coupling, but then those not in direct contact with the probe relax, producing an artifactual adaptation (see also *Materials and Methods*). Indeed, it has been demonstrated that when the vertical positioning of the rigid probe was not optimal in respect to the bundle of cochlear OHCs, it produced an artifactually large and Ca^{2+}-independent MET current decay (25), similar to that observed in ref. 19. This technical constraint is not an issue when stimulating the hair bundles of lower-vertebrate or mammalian vestibular hair cells because of their more compact structure, which allows for better coupling with a rigid probe (7, 8, 24, 38). In the mammalian cochlea, the stimulus produced by the fluid jet allows a more uniform displacement of the whole hair bundle (Fig. S1) and is sufficiently fast to allow submillisecond decay time-constants of MET current adaptation to be observed. A particularly strong argument for Ca^{2+}-dependent adaptation that in principle does not depend on the method of bundle stimulation is the increase in resting open probability of the MET current in low extracellular Ca^{2+}, with strong BAPTA buffering, or at depolarized potentials. Our results show that the long-standing theory implicating Ca^{2+} ion entry through the MET channels as the main regulator of adaptation in lower-vertebrate hair cells also applies to the hair cells of the mammalian cochlea.

Materials and Methods

Electrophysiology. OHCs ($n = 92$) and IHCs ($n = 30$) from the mouse cochlea were studied in acutely dissected organs of Corti from P4 to P9, where the day of birth is P0. Animals of either sex were killed by cervical dislocation, under Schedule 1 in accordance with UK Home Office regulations and approved by the University of Sheffield Ethical Review Committee. Cochleae were dissected as described (23, 39). Whole-cell patch-clamp recordings were performed at room temperature (22–24 °C). Statistical comparisons of means were made by Student's two-tailed *t* test (paired or unpaired, as appropriate), and for multiple comparisons, ANOVA, one-way ANOVA followed by the Tukey test. Mean values are shown ± SEM where $P < 0.05$ indicates statistical significance. See *SI Materials and Methods* for more details.

Hair Bundle Stimulation. MET currents were elicited by stimulating the hair bundles of hair cells using a fluid jet from a pipette driven by a piezoelectric disk (20–23). The pipette was pulled from borosilicate glass to a final overall length of 5.3–5.5 cm. The pipette tip (diameter 7–10 μm) was positioned at ∼8 μm from the bundles of hair cells (Fig. S1 *A* and *B*). The width of the hair bundle was: 6.7 ± 0.1 μm ($n = 10$) for OHCs and 8.7 ± 0.4 μm ($n = 10$) for IHCs. The height of the OHC bundles was 4.3 ± 0.3 μm ($n = 12$); this measure was used to assess bundle stiffness (Fig. S2) as described (21). Mechanical stimuli were applied as 20- or 50-ms steps, paired-pulse steps, or 45- or 50-Hz sinusoids (filtered at 1 kHz, 8-pole Bessel) with driving voltages of up to ±40 V. In most cases, the jet was placed on the modiolar side of the bundle (with the patch pipette placed opposite), but in a few experiments performed on IHCs (7 of 30), the position of fluid jet and patch pipette was swapped. This different bundle stimulation approach has been described and produces comparable responses (40), as expected given the linear behavior of the fluid jet (Fig. S2). Before the positioning of the fluid jet by the hair bundles, any steady-state pressure was removed by monitoring the movement of debris in front of the pipette.

Whereas IHC bundles are believed to be stimulated in vivo by fluid motion, making the fluid jet approach the most suitable stimulus in vitro, those of OHCs are coupled to the tectorial membrane with the consequence that neither of the methods of stimulation currently used to displace the hair bundle (fluid jet and stiff probe) are able to reproduce the in vivo condition (16). Both the fluid jet and stiff probe have potential limitations: The probe is unlikely to contact all stereocilia rows, especially those at the center and two edges of the V-shaped bundles, causing their nonuniform deflection; the stimulus applied by the fluid jet can be slower than that achievable with a glass probe (16, 24). Although the fluid jet can produce slower bundle movements (17, 19), with consequences for the adaptation time constants

(24), our in-house–built fluid jet system allows the recording of submillisecond MET current adaptation (10–90% rise time for the nonadapting MET current in OHCs; 0.50 ± 0.02 ms; $n = 16$). We investigated whether the hair bundles of OHCs and IHCs were displaced uniformly during fluid-jet step stimulation by imaging them using a fast camera (ORCA Flash 4; Hamamatsu). We found that in both cell types, the hair bundle movement is spatially uniform across their width using our fluid jet system (Fig. S1 *C–F*).

The conversion value used to express the piezo-driver voltage into displacement at the top of the OHC hair bundle was obtained by using a photodiode system. The fluid jet was calibrated by using carbon fibers of a uniform diameter of 8 μm (Fig. S2*A*) and 10 μm (Fig. S2*B*) placed at the bottom of the recording chamber and at a similar distance (~7.5 μm) from the pipette tip of the fluid jet as for the hair bundle. The carbon fiber displacement traces (Fig. S2 *A* and *B*, *Middle*) show that the force/pressure from the fluid jet to the bundle remains constant during a step stimulus. The force from the fluid jet applied to the OHC bundle has been calculated as described (21) and was 7.7×10^{-11} and 10.3×10^{-11} N per volt of the driver voltage for Fig. S2 *A* and *B*, respectively. Bundle motion during fluid jet stimulation was determined by projecting an image of the OHC bundle onto a pair of photodiodes (LD 2-5; Centronics) at 360× total magnification as described (22). The differential photocurrent was filtered at 5 kHz and was calibrated by measuring its amplitude when displacing the photodiodes a known amount in the image plane and then using the magnification to determine the equivalent motion in the object plane. In some experiments, bundle movements were recorded with a laser differential interferometer (21). The conversion value used to express the piezo-driver voltage into displacement at the top of the OHC hair bundle for most of the MET current recordings was obtained from a sample of 12 recordings from P5–P8 OHCs (10.1 nm/V: Fig. S2 *C* and *D*). Fig. S3 also shows an example where MET currents and OHC bundle displacements were measured simultaneously.

ACKNOWLEDGMENTS. This work was supported by Wellcome Trust Grant 091895 (to W.M.), a Medical Research Council grant (to C.J.K.), and a Royal Society grant (to S.L.J.). S.L.J. is a Royal Society University Research Fellow.

1. Beurg M, Fettiplace R, Nam JH, Ricci AJ (2009) Localization of inner hair cell mechanotransducer channels using high-speed calcium imaging. *Nat Neurosci* 12(5):553–558.
2. Fettiplace R, Hackney CM (2006) The sensory and motor roles of auditory hair cells. *Nat Rev Neurosci* 7(1):19–29.
3. Schwander M, Kachar B, Müller U (2010) Review series: The cell biology of hearing. *J Cell Biol* 190(1):9–20.
4. Pickles JO, et al. (1989) The organization of tip links and stereocilia on hair cells of bird and lizard basilar papillae. *Hear Res* 41(1):31–41.
5. Tilney LG, Tilney MS, DeRosier DJ (1992) Actin filaments, stereocilia, and hair cells: How cells count and measure. *Annu Rev Cell Biol* 8:257–274.
6. Corey DP, Hudspeth AJ (1983) Kinetics of the receptor current in bullfrog saccular hair cells. *J Neurosci* 3(5):962–976.
7. Eatock RA, Corey DP, Hudspeth AJ (1987) Adaptation of mechanoelectrical transduction in hair cells of the bullfrog's sacculus. *J Neurosci* 7(9):2821–2836.
8. Howard J, Hudspeth AJ (1987) Mechanical relaxation of the hair bundle mediates adaptation in mechanoelectrical transduction by the bullfrog's saccular hair cell. *Proc Natl Acad Sci USA* 84(9):3064–3068.
9. Assad JA, Hacohen N, Corey DP (1989) Voltage dependence of adaptation and active bundle movement in bullfrog saccular hair cells. *Proc Natl Acad Sci USA* 86(8):2918–2922.
10. Crawford AC, Evans MG, Fettiplace R (1989) Activation and adaptation of transducer currents in turtle hair cells. *J Physiol* 419:405–434.
11. Holt JR, Corey DP, Eatock RA (1997) Mechanoelectrical transduction and adaptation in hair cells of the mouse utricle, a low-frequency vestibular organ. *J Neurosci* 17(22):8739–8748.
12. Ricci AJ, Fettiplace R (1998) Calcium permeation of the turtle hair cell mechanotransducer channel and its relation to the composition of endolymph. *J Physiol* 506(Pt 1):159–173.
13. Wu YC, Ricci AJ, Fettiplace R (1999) Two components of transducer adaptation in auditory hair cells. *J Neurophysiol* 82(5):2171–2181.
14. Eatock RA (2000) Adaptation in hair cells. *Annu Rev Neurosci* 23:285–314.
15. Waguespack J, Salles FT, Kachar B, Ricci AJ (2007) Stepwise morphological and functional maturation of mechanotransduction in rat outer hair cells. *J Neurosci* 27(50):13890–13902.
16. Fettiplace R, Kim KX (2014) The physiology of mechanoelectrical transduction channels in hearing. *Physiol Rev* 94(3):951–986.
17. Kennedy HJ, Evans MG, Crawford AC, Fettiplace R (2003) Fast adaptation of mechanoelectrical transducer channels in mammalian cochlear hair cells. *Nat Neurosci* 6(8):832–836.
18. Lelli A, Asai Y, Forge A, Holt JR, Géléoc GS (2009) Tonotopic gradient in the developmental acquisition of sensory transduction in outer hair cells of the mouse cochlea. *J Neurophysiol* 101(6):2961–2973.
19. Peng AW, Effertz T, Ricci AJ (2013) Adaptation of mammalian auditory hair cell mechanotransduction is independent of calcium entry. *Neuron* 80(4):960–972.
20. Kros CJ, Rüsch A, Richardson GP (1992) Mechano-electrical transducer currents in hair cells of the cultured neonatal mouse cochlea. *Proc Biol Sci* 249(1325):185–193.
21. Géléoc GSG, Lennan GWT, Richardson GP, Kros CJ (1997) A quantitative comparison of mechanoelectrical transduction in vestibular and auditory hair cells of neonatal mice. *Proc Biol Sci* 264(1381):611–621.
22. Johnson SL, Beurg M, Marcotti W, Fettiplace R (2011) Prestin-driven cochlear amplification is not limited by the outer hair cell membrane time constant. *Neuron* 70(6):1143–1154.
23. Johnson SL, Kennedy HJ, Holley MC, Fettiplace R, Marcotti W (2012) The resting transducer current drives spontaneous activity in prehearing mammalian cochlear inner hair cells. *J Neurosci* 32(31):10479–10483.
24. Vollrath MA, Eatock RA (2003) Time course and extent of mechanotransducer adaptation in mouse utricular hair cells: Comparison with frog saccular hair cells. *J Neurophysiol* 90(4):2676–2689.
25. Indzhykulian AA, et al. (2013) Molecular remodeling of tip links underlies mechanosensory regeneration in auditory hair cells. *PLoS Biol* 11(6):e1001583.
26. Karavitaki KD, Corey DP (2014) A new probe for cochlear hair bundle stimulation. *Assoc Res Otolaryngol. Abstract* SY-079:440.
27. Ohmori H (1985) Mechano-electrical transduction currents in isolated vestibular hair cells of the chick. *J Physiol* 359:189–217.
28. Crawford AC, Evans MG, Fettiplace R (1991) The actions of calcium on the mechano-electrical transducer current of turtle hair cells. *J Physiol* 434:369–398.
29. Beurg M, Nam JH, Chen Q, Fettiplace R (2010) Calcium balance and mechanotransduction in rat cochlear hair cells. *J Neurophysiol* 104(1):18–34.
30. Marcotti W, van Netten SM, Kros CJ (2005) The aminoglycoside antibiotic dihydrostreptomycin rapidly enters mouse outer hair cells through the mechano-electrical transducer channels. *J Physiol* 567(Pt 2):505–521.
31. Steel KP, Barkway C (1989) Another role for melanocytes: Their importance for normal stria vascularis development in the mammalian inner ear. *Development* 107(3):453–463.
32. Bosher SK, Warren RL (1971) A study of the electrochemistry and osmotic relationships of the cochlear fluids in the neonatal rat at the time of the development of the endocochlear potential. *J Physiol* 212(3):739–761.
33. Ricci AJ, Fettiplace R (1997) The effects of calcium buffering and cyclic AMP on mechano-electrical transduction in turtle auditory hair cells. *J Physiol* 501(Pt 1):111–124.
34. Assad JA, Corey DP (1992) An active motor model for adaptation by vertebrate hair cells. *J Neurosci* 12(9):3291–3309.
35. Stauffer EA, Holt JR (2007) Sensory transduction and adaptation in inner and outer hair cells of the mouse auditory system. *J Neurophysiol* 98(6):3360–3369.
36. He DZ, Jia S, Dallos P (2004) Mechanoelectrical transduction of adult outer hair cells studied in a gerbil hemicochlea. *Nature* 429(6993):766–770.
37. Kawashima Y, et al. (2011) Mechanotransduction in mouse inner ear hair cells requires transmembrane channel-like genes. *J Clin Invest* 121(12):4796–4809.
38. Crawford AC, Fettiplace R (1985) The mechanical properties of ciliary bundles of turtle cochlear hair cells. *J Physiol* 364:359–379.
39. Zampini V, et al. (2013) Burst activity and ultrafast activation kinetics of CaV1.3 Ca^{2+} channels support presynaptic activity in adult gerbil hair cell ribbon synapses. *J Physiol* 591(Pt 16):3811–3820.
40. Zampini V, et al. (2011) Eps8 regulates hair bundle length and functional maturation of mammalian auditory hair cells. *PLoS Biol* 9(4):e1001048.